Iraqi Journal of Science, 2024, Vol. 65, No. 7, pp: 3754-3764
DOI: 10.24996/ijs.2024.65.7.16

ISSN: 0067-2904

Effect of Manganese Oxide Doping of Tin Oxide Thin Films on the Optical and Structural Properties

Sara S. Mahmood [1*], Bushra A. Hasan [2], Aws F. Rauuf [3]
[1]*Renewable directorate, ministry of science and technology, Baghdad, Iraq*
[2]*Department of Physics, College of Science, University of Baghdad, Baghdad, Iraq*
[3]*Material directorate, ministry of science and technology, Baghdad, Ira*

Received: 19/10/2022 Accepted: 12/6/2023 Published: 30/7/2024

Abstract:
Tin oxide pure and manganese oxide doped (SnO_2:Mn_2O_3) films were grown on a glass substrate in vacuum by pulsed laser deposition (PLD) technique (using Nd: YAG Laser) at different ratios of Mn_2O_3 (0, 3, 5, 7, 9) % wt. The structural and optical properties were studied. The X-ray diffraction (XRD) studies showed the structure nature of the films to be polycrystalline and rutile tetragonal. The optical transmittance spectra and optical constants of the prepared thin films, such as extinction coefficient (k), refractive index (n), and real (ε_r) and imaginary parts (ε_i) of the dielectric constant, were investigated. The values of the energy band gap increased from 3.5 eV to 3.55 eV with increasing the doping concentration.

Keywords: pulse laser deposition, tin oxide, Optical properties.

تأثير ذرات أوكسيد المنغنيز على الخواص البصرية والتركيبية لأغشية أوكسيد القصدير الرقيقة

سارة صادق محمود[1*]، بشرى عباس حسن[2]، اوس فيصل رؤوف[3]
[1] دائرة الطاقات المتجددة، وزارة العلوم والتكنولوجيا، بغداد، العراق.
[2] قسم الفيزياء، كلية العلوم، جامعة بغداد، بغداد، العراق.
[3] دائرة بحوث المواد، وزارة العلوم والتكنولوجيا، بغداد، العراق.

الخلاصة:
تم ترسيب أغشية رقيقة من أوكسيد القصدير النقي والمشوب بأوكسيد المنغنيز (SnO_2: Mn_2O_3) على قواعد زجاجية وبنسب وزنية مختلفة (0، 3، 5، 7، 9) ٪ بتقنية الترسيب بالليزر النبضي (PLD) باستخدام ليزر Nd: YAG. تمت دراسة الخصائص التركيبية والبصرية للأغشية المحضرة حيث أظهرت دراسة حيود الأشعة السينية (XRD) أن الأغشية متعددة التبلور بتركيب رباعي قائم الزاوية كذلك فحص لها طيف النفاذية الضوئية والثوابت البصرية مثل معامل الخمود (k) ومعامل الانكسار (n) والجزء الخيالي (ε_i) والجزء الحقيقي (ε_r) من ثابت العزل الكهربائي. ولوحظ ان قيم فجوة الطاقة تزداد بزيادة تركيز الشوائب من 3.5 فولت إلى 3.55 فولت.

Introduction

Tin dioxide (SnO_2) films are n-type semiconductor materials with a wide energy gap band (3.7 eV) [1]. The study of SnO_2 thin film is of great interest due to its attractive features such

*Email: aws.raouf1104@sc.uobaghdad.edu.iq

as uniformity, good optical properties, electrical properties, chemical properties, mechanical hardness, heat treatment stability, and low cost. [1-4]. There are many deposition methods used to prepare SnO_2 films. Pulsed Laser Deposition (PLD) is one of the most effective physical methods to produce nanoparticles with high quality, low cost, single step, and no contamination. PLD is used to accomplish high-quality SnO_2 thin films. [5-8]. Metal oxides (e.g., MnO_2, Fe_2O_3, RuO_2, and VO) offer high pseudo capacitance through fast and reversible redox reactions near the surface of active materials [9]. Manganese oxide is important among such oxide materials because of its attractive high specific capacity, non-toxicity in conjunction with its earth abundance, and environmentally compatible. (Mn) is a transition metal with oxidation states (+4, +3, +2) and can give several phases of manganese oxides such as Mn_5O_8, Mn_3O_4, Mn_2O_3, MnO_2, and MnO. The most common and stable manganese dioxides in nature are mineral pyrolusite β-MnO_2. It has a simple rutile tetragonal structure known as the mineral Hausmannite at ambient air temperature and a distorted spinel structure [10-11].

Sabri et al. [12] reported the influence of Mn doping on the structural and optical properties of SnO_2 nanoparticles. The crystallite size was found to be 24 to 35 nm. Singh et al. [13] prepared MnO_2-SnO_2 nanocomposite as a sensing device for liquefied petroleum gas (LPG). X-ray diffraction pattern proved that the material is highly crystalline with an average crystallite size of 16.786 nm with a cubic phase manganese oxide and tetragonal tin oxide. The energy band gap values were 3.407 eV, 3.037 eV, and 3.202 eV for MnO_2, SnO_2, and MnO_2-SnO_2, respectively. Hussein et al. [14] fabricated (PEO-PVP) blend doped with SnO_2/MnO_2NPs for photodegradation of organic pollutants with low cost, high activity, high propagation and anti-aggregation of nanoparticles compared with other materials. The results indicated that the absorbance of the (PEO–PVP) blend increases by about 51% with the addition of 4.5 MnO_2 NPs.

This work is concerned with the synthesis of manganese oxide doped tin oxide with various doping ratios. It explores the role of doping ratio on the microstructure of the prepared thin film samples and its optical properties. The main goal of this work is to produce good properties in SnO_2: Mn_2O_3 based systems.

Experimental Procedure

SnO_2 and SnO_2: Mn_2O_3 films with different doping ratios (0, 3, 5, 7, 9) % wt. were prepared by the PLD technique on (2.5× 8 cm^2) glass substrates of 1 mm thickness. The glass substrates were cleaned with a methanol solution in an ultrasonic bath for 30 min. Thin films were deposited using (Nd: YAG) laser of (1064 nm) wavelength with a fluency of (400-700 mJ/cm^2). SnO_2 and Mn_2O_3 powder (supplied by Sigma-Aldrich) were pressed into pellets of (1 cm) diameter by uniaxial pressure (~0.8 MPa). The Pellets were the target in the system placed (1 cm) away from the substrate. The thin films were analyzed with an X-ray diffractometer (Siemens D-5000) for their structural properties. The optical properties of the films were studied by a UV-Vis spectrometer (OPTIMA SP-3000) at the wavelength range of (300- 1100) nm at room temperature.

Results and discussion :

The XRD patterns, shown in Figure (1), demonstrate the crystal structure of SnO_2:Mn_2O_3 thin films, of t≈150 nm thickness, deposited on the glass substrates at different ratios of Mn_2O_3 (0, 3, 5, 7, 9) % wt. The (d) spacing was calculated from the following equation (Brag law):

$$2d \sin\theta = n\lambda \quad \dots (1)$$

Where: λ is the wavelength (λ=1.5406Å from Cu-Kα source), n is an integer and θ is diffraction angle (Bragg angle) in radian.

The crystal size D for each XRD peak was calculated using Scherrer equation [15]:

$$D = \frac{0.94\lambda}{\beta\cos\theta} \quad \ldots (2)$$

Where: β is the Full Width at Half Maximum (FWHM) of the XRD peaks.

The dislocation density (δ) and the micro strain train (έ) were measured using the following equations:

$$\delta = \frac{1}{D^2} \quad \ldots (3)$$

$$\acute{\varepsilon} = \frac{\beta\cos\theta}{4} \quad \ldots (4)$$

The diffraction peaks were indexed and retrieved by the JCPDS standard data (No. 88-0287). All the films were polycrystalline and had a tetragonal structure. The most intense peaks were located at 2θ=26.8137, 34.1176, 38.1618, 39.1667, 51.9853, 54.9510, 58.0392, 62.0833, 64.9510, 66.1765 degrees corresponding to the planes (110), (101), (200), (111), (211), (220), (002), (310), (112) and (301), respectively. This result agrees with other reported studies [16,18].

There was no trace of impurities phase of manganese in the oxide XRD patterns at (3, 5 and 7) % doping ratios, which agrees with the results of Sharma and Sharma [19]. But impurities were detected at 9% doping ratio for the diffraction peaks at 2θ=33.1863 corresponding to the (222) plane. The result agrees with JCPDS (card No. 89-4836) [10].

The peaks of the XRD patterns were observed to be shifted towards higher angles when increasing the MnO_2 ratio indicating that the Mn ions have substituted the Sn positions without changing the rutile structure [20]. The crystallite size decreased with the introduction of the MnO_2 dopant because the growth of the crystal grains was inhibited, resulting in the existence of Mn ions in SnO_2. The oxygen vacancies increased with MnO_2 doping because the ionic radius of Mn^{3+} ions of 0.65 A^o is smaller than that of Sn^{4+} ions of 0.69 A^o. Hence, the crystallite size decrease is due to the disturbance in the long-range crystallographic ordering [19,21,22].

Figure 1: The XRD pattern of SnO_2 and SnO_2: Mn_2O_3 thin films at different doping ratios.

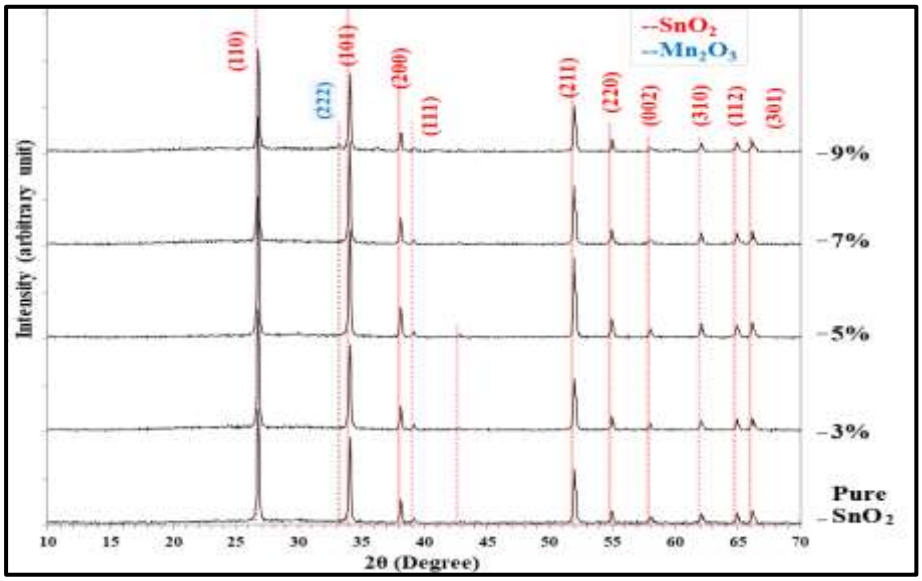

Table 1: Structural parameters of SnO_2 and SnO_2: Mn_2O_3 thin films at different doping ratios.

Mn%	2θ (Deg.)	FWHM (Deg.)	d_{hkl} (Å)	D (nm)	hkl	Phase	$\delta \times 10^{15}$ (line/m^2)	$\varepsilon \times 10^{-3}$
Pure	26.8137	0.1716	3.3222	47.6	(110)	SnO_2	0.44	0.73
	34.1176	0.2206	2.6258	37.7	(101)	SnO_2	0.70	0.92
	38.1618	0.2451	2.3564	34.3	(200)	SnO_2	0.85	1.01
	39.1667	0.2696	2.2982	31.3	(111)	SnO_2	1.02	1.11
	51.9853	0.2451	1.7576	36.1	(211)	SnO_2	0.77	0.96
	54.9510	0.2450	1.6696	36.6	(220)	SnO_2	0.75	0.95
	58.0392	0.3431	1.5879	26.5	(002)	SnO_2	1.43	1.31
	62.0833	0.2941	1.4938	31.5	(310)	SnO_2	1.01	1.10
	64.9510	0.2696	1.4346	34.9	(112)	SnO_2	0.82	0.99
	66.1765	0.3187	1.4110	29.8	(301)	SnO_2	1.13	1.17
3	26.8137	0.1961	3.3222	41.7	(110)	SnO_2	0.58	0.83
	34.0931	0.2206	2.6277	37.7	(101)	SnO_2	0.70	0.92
	38.1618	0.2206	2.3564	38.1	(200)	SnO_2	0.69	0.91
	39.1912	0.1961	2.2968	43.0	(111)	SnO_2	0.54	0.81
	52.0098	0.2696	1.7569	32.8	(211)	SnO_2	0.93	1.06
	54.9510	0.2205	1.6696	40.6	(220)	SnO_2	0.61	0.85
	58.0882	0.1961	1.5867	46.4	(002)	SnO_2	0.47	0.75
	62.0833	0.2696	1.4938	34.4	(310)	SnO_2	0.84	1.01
	64.9755	0.2696	1.4341	34.9	(112)	SnO_2	0.82	0.99
	66.1520	0.2451	1.4114	38.7	(301)	SnO_2	0.67	0.90
5	26.7892	0.1961	3.3252	41.7	(110)	SnO_2	0.58	0.83
	34.0931	0.2451	2.6277	33.9	(101)	SnO_2	0.87	1.02
	38.1618	0.2451	2.3564	34.3	(200)	SnO_2	0.85	1.01
	39.1667	0.2451	2.2982	34.4	(111)	SnO_2	0.84	1.01
	51.9608	0.2451	1.7584	36.1	(211)	SnO_2	0.77	0.96
	54.9510	0.2696	1.6696	33.2	(220)	SnO_2	0.91	1.04
	58.0147	0.2206	1.5885	41.2	(002)	SnO_2	0.59	0.84
	62.1078	0.2206	1.4933	42.1	(310)	SnO_2	0.57	0.82
	64.9510	0.3677	1.4346	25.6	(112)	SnO_2	1.52	1.35
	66.1520	0.2941	1.4114	32.2	(301)	SnO_2	0.96	1.08
7	26.7892	0.1961	3.3252	41.7	(110)	SnO_2	0.58	0.83
	34.0686	0.2206	2.6295	37.7	(101)	SnO_2	0.70	0.92
	38.1618	0.1961	2.3564	42.9	(200)	SnO_2	0.54	0.81
	39.1667	0.2206	2.2982	38.2	(111)	SnO_2	0.68	0.91
	51.9608	0.2451	1.7584	36.1	(211)	SnO_2	0.77	0.96
	54.9510	0.2450	1.6696	36.6	(220)	SnO_2	0.75	0.95
	58.0392	0.2941	1.5879	30.9	(002)	SnO_2	1.05	1.12
	62.0833	0.2696	1.4938	34.4	(310)	SnO_2	0.84	1.01
	64.9755	0.2941	1.4341	32.0	(112)	SnO_2	0.97	1.08
	66.1765	0.2696	1.4110	35.2	(301)	SnO_2	0.81	0.99
9	26.8137	0.1961	3.3222	41.7	(110)	SnO_2	0.58	0.83
	33.1863	0.3432	2.6974	24.2	(222)	Mn_2O_3	1.71	1.44
	34.1176	0.2206	2.6258	37.7	(101)	SnO_2	0.70	0.92
	38.1618	0.1961	2.3564	42.9	(200)	SnO_2	0.54	0.81
	39.1912	0.2451	2.2968	34.4	(111)	SnO_2	0.84	1.01
	51.9853	0.2451	1.7576	36.1	(211)	SnO_2	0.77	0.96
	54.9510	0.2206	1.6696	40.6	(220)	SnO_2	0.61	0.85
	57.9902	0.2696	1.5891	33.7	(002)	SnO_2	0.88	1.03
	62.1078	0.2696	1.4933	34.4	(310)	SnO_2	0.84	1.01
	64.9510	0.2941	1.4346	32.0	(112)	SnO_2	0.97	1.08
	66.1520	0.3187	1.4114	29.8	(301)	SnO_2	1.13	1.17

The values of lattice contents a and c were measured according to the relation:

$$\frac{1}{d} = \frac{h^2 + k^2}{a^2} + \frac{l^2}{c^2} \quad \ldots (5)$$

Table 2: The values of lattice contents of SnO_2 and SnO_2: Mn_2O_3 films at different doping ratios.

Mn%	a (Å)	c (Å)
0	4.69830	3.17578
3	4.69830	3.17334
5	4.70252	3.17701
7	4.70252	3.17578
9	4.69830	3.17823

The value of d spacing belonging to the (110) plane was found to increase with the increase of the doping ratio reflecting growth in lattice parameters by increasing the Mn_2O_3 ratio, as seen in Table 2. This result was also found by Sharma et al. [23]. This behavior is expected due to the difference in the ionic radii of Sn and Mn ions. The FWHM values belong to the [110] plane of SnO_2, pointed out a reduction of crystallinity accompanying the insertion of Mn^{+3} ions in the oxide lattice, as shown in Table 1. The growth of the microstrain, as shown in the same table, causes the reduction of crystallite size.

It is evident that no traces of Mn_2O_3 were detected in the XRD patterns at low doping concentrations (0, 3, 5 and 7 %). Tiny peak was observed at a high doping ratio of 9% located at $2\theta=33.18^o$ corresponding to (222) plane.

The UV- Visible transmittance of the SnO_2 and SnO_2: Mn_2O_3 thin films with different doping ratios (0, 3, 5, 7 and 9%) was measured using (OPTIMA SP-3000) spectrophotometer at wavelength 300-1100 nm. Figure (2) shows maximum transmittance at a doping ratio of 9% .

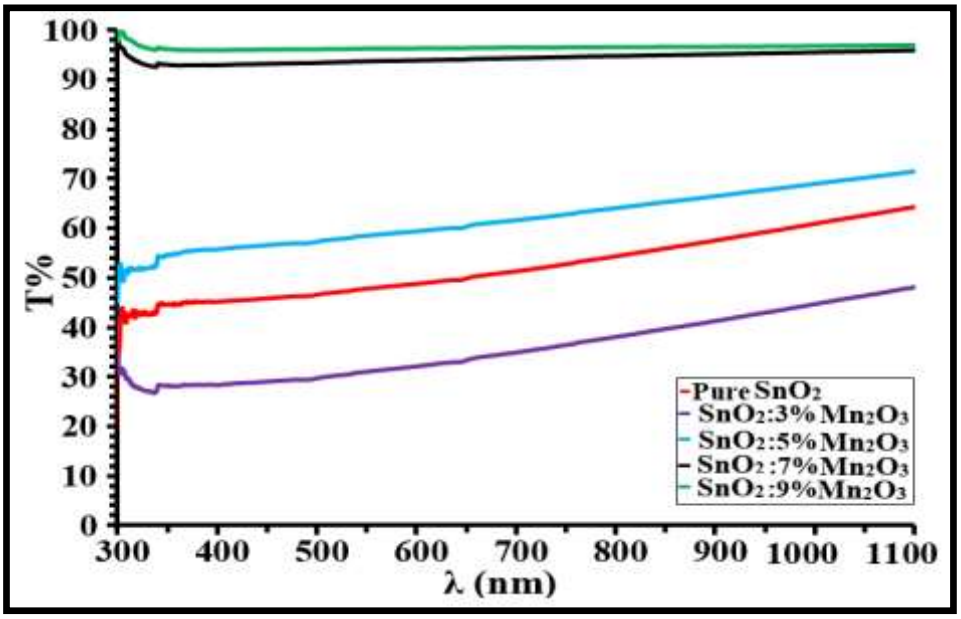

Figure 2: Transmittance spectra of SnO_2 and SnO_2: Mn_2O_3 films at different doping ratios.

The increase in transmittance accompanied the increase in the doping ratio from 3 to 9%wt, as shown in Table (3). The increasing in Mn_2O_3 ratio made the prepared films more opaque or

less transparent (lowering the absorption coefficient), which is reflected by the shift of the absorption edge toward higher values of energy [21].

A relation between the coefficient of absorption α and incident photon energy hν can be illustrated by Equations (6) and (7) [25,26]:

$$\alpha = 2.303 \frac{A}{t} \quad \ldots (6)$$

Where: A is the absorbance and t is the thickness of the film .
The optical energy gap E_g was measured from Tauc relation:

$$(\alpha h\nu)^2 = B\,(h\nu - E_g) \quad \ldots (7)$$

Where: h is Planck's constant, ν is the frequency of the incident light, and B is a constant. The optical energy band gap values (E_g) for SnO_2 and SnO_2: Mn_2O_3 films were calculated depending on the absorption spectra. Plots of $(\alpha h\nu)^2$ versus hν for thin films for the different doping ratios, shown in Figures (3) and (4), were linear, indicating the direct band gap nature of the films. Extrapolating the line to the hν axis gives the band gap energy, as given in Table 3. The value E_g of SnO_2 thin film is (3.5eV), which agrees with the result of Sharma and Sharma [19]. A doping ratio of 3% decreased the band gap energy to about 3.4 eV; this decrease can result in the dopant atoms to the formation of donor levels within the energy gap near the conduction band. Thus, a thin film sample will absorb photons at low energy. The E_g at other ratios increases with Mn_2O_3 doping, achieving a maximum value of 3.55 eV at 9%.

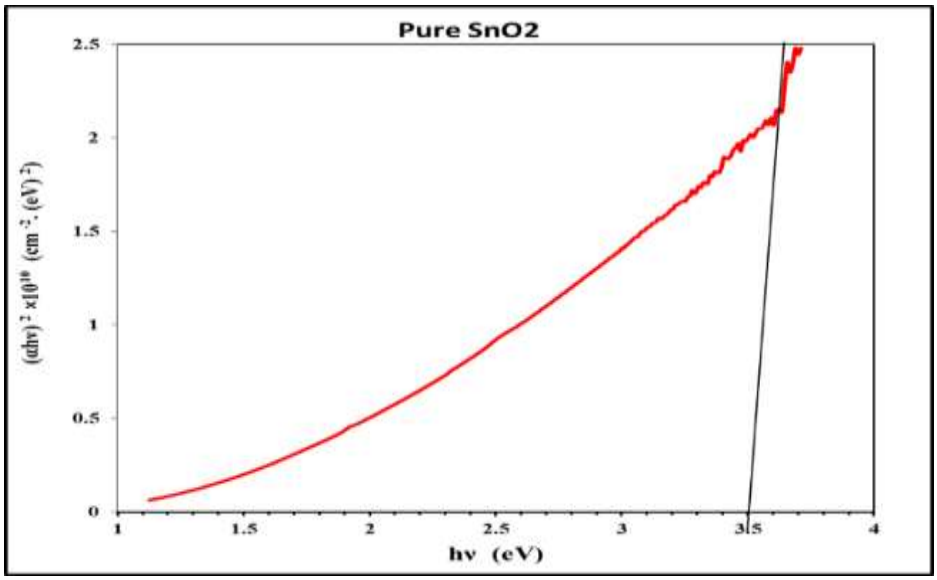

Figure 3: Optical band gap of SnO_2 films grown on glass substrates.

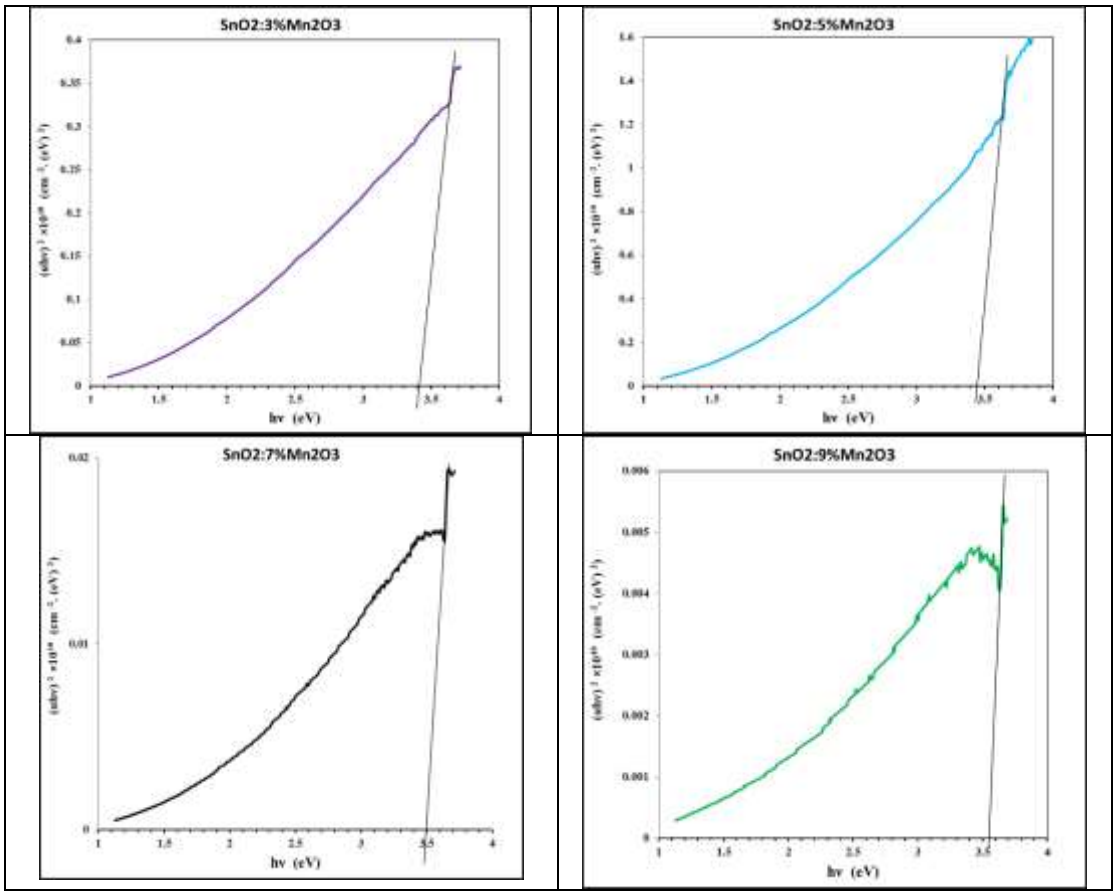

Figure 4: Optical band gap of SnO_2: Mn_2O_3 films at different doping ratios.

The increase of the energy band gap by increasing the doping ratio (Mn_2O_3 content), which can be explained according to the Burstein-Moss (BM) effect, is ascribed to the increase in carrier concentration. In heavily doped semiconductors, excess electrons occupy levels near the conduction band. As optical transitions are vertical in SnO_2 and Pauli Exclusion Principle restricts states to be singly occupied, valence electrons need additional energy to be excited to higher states in the conduction band. According to Burstein, the magnitude of Burstein-Moss shift $(\Delta E)_{BM}$ in the energy gap defined as the shift of Fermi level with respect to the bottom of the conduction band, can be approximated using the relation [20,25]:

$$\Delta E_{BM} = \frac{2}{2m*}(2\pi^2 \bar{n})^{3/2} \quad \ldots (8)$$

Where: m* is the electron effective mass, and $\bar{n}$ is the electron density determined from Hall effect measurements .

Optical constants, such as refractive index (n), extinction coefficient (k), and real (ε_r) and imaginary parts (ε_i) of dielectric constant were calculated [26,27].

$$k = \frac{\alpha\lambda}{4\pi} \quad \ldots (9)$$

$$\varepsilon_r = n^2 - k^2 \quad \ldots (10)$$

$$\varepsilon_i = 2nk \quad \ldots (11)$$

$$n = \left[\frac{4R}{(R-1)^2} - k^2\right] 1/2 - \frac{(R+1)}{(R-1)} \quad \ldots (12)$$

$$R=\frac{(n-1)^2+k^2}{(n+1)^2k^2} \quad \ldots (13)$$

Where: R is the reflectance. It can be noticed from Figure (5) and Table (3) that (n) generally decreased with the doping concentration. The behavior of the refractive index can be explained that the addition of Mn_2O_3 leads to the decrease of the packing density of SnO_2, which in turn increases the propagation velocity of light through the sample resulting in the decrease in the values of (n), where (n) represents the ratio of light velocity in vacuum to velocity through the medium [28].

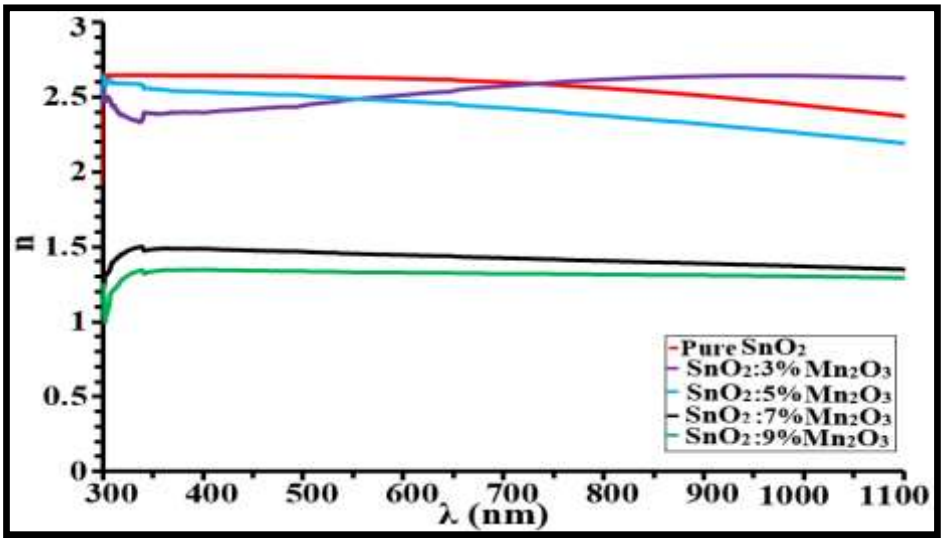

Figure 5: Variation of the refractive index of SnO_2 and SnO_2: Mn_2O_3 films at different doping ratios with wavelength.

The extinction coefficient (k) behavior is shown in Figure (6). The extinction coefficients values decrease due to absorption and grain scattering [18]. In addition, if the increase of the Mn_2O_3 ratio reduces the absorption coefficient or absorbance, k is reduced .

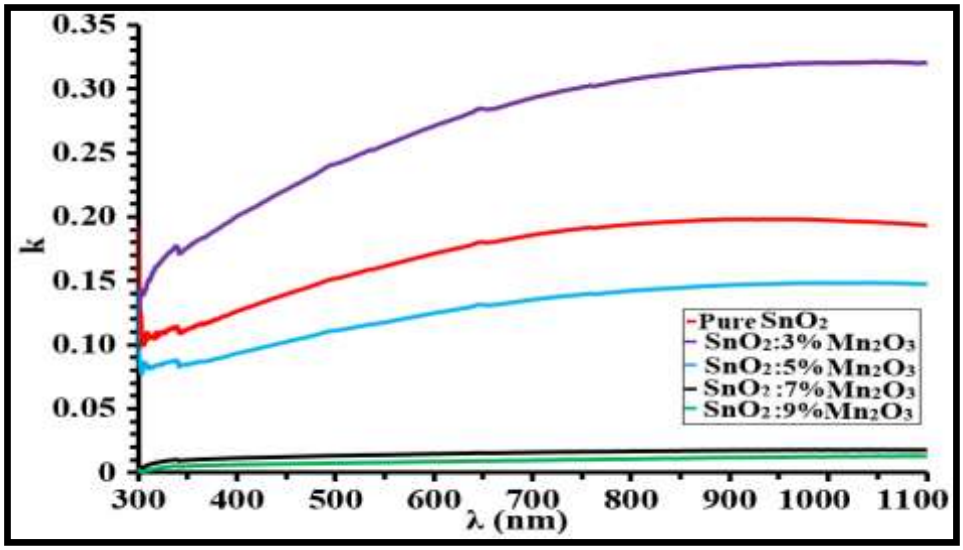

Figure 6: Variation of the extinction coefficient of SnO_2 and SnO_2: Mn_2O_3 films at different doping ratios with wavelength.

The spectral distribution of ε_r and ε_i are shown in Figures (7) and (8). It is obvious that ε_r and ε_i exhibit the same manner as n and k, respectively, and the same explanation can be given.

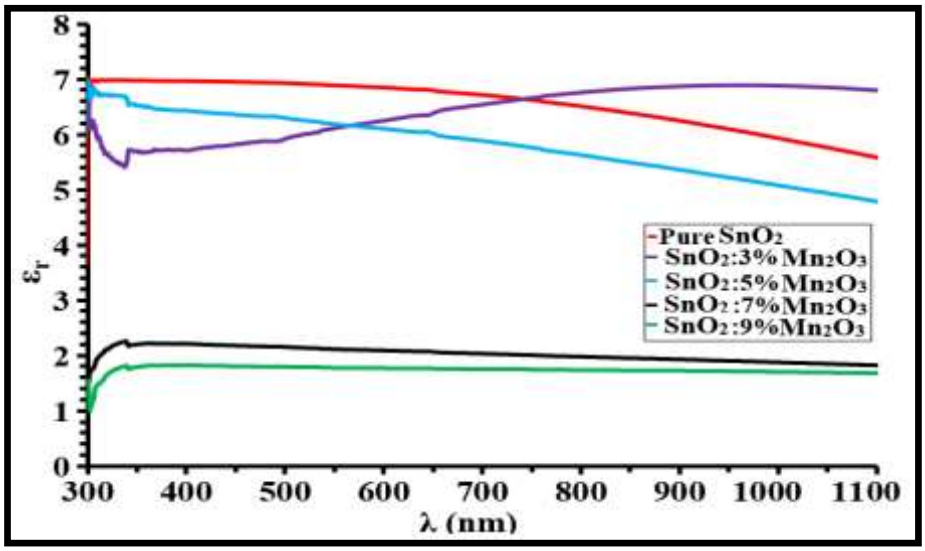

Figure 7: Variation of the real part of the dielectric constant of SnO_2 and SnO_2: Mn_2O_3 films at different doping ratios with wavelength.

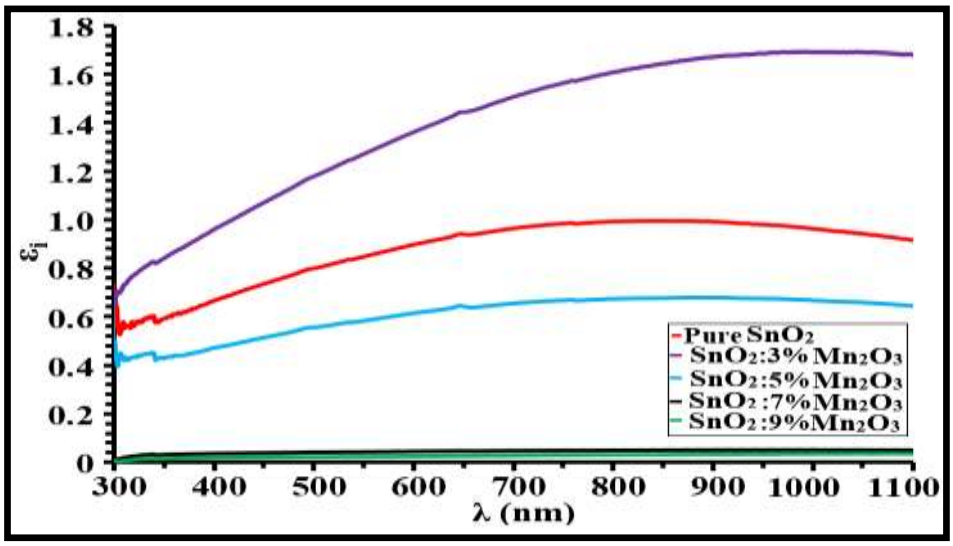

Figure 8: Variation of the imaginary part of the dielectric constant of SnO_2 and SnO_2: Mn_2O_3 films at different doping ratios with wavelength.

Table 3: optical parameters of SnO_2 and SnO_2: Mn_2O_3 films with different doping ratios at λ=550 nm.

Mn%	T%	α (cm^{-1})	k	n	ε_r	ε_i	E_g (eV)
0	47.81	36906	0.162	2.628	6.883	0.850	3.50
3	74.64	14624	0.064	2.104	4.424	0.270	3.40
5	58.48	26830	0.117	2.490	6.184	0.585	3.45
7	93.81	3195	0.014	1.453	2.112	0.041	3.50
9	96.38	1842	0.008	1.331	1.772	0.021	3.55

Conclusion:

Pure SnO_2 and doped SnO_2: Mn_2O_3 thin films of different doping ratios (0, 3, 5, 7, 9) % wt. deposited on glass substrates were prepared at ambient temperature using the pulsed laser deposition technique. The structure of SnO_2: Mn_2O_3 was studied by XRD, which indicates the best crystalline in a tetragonal structure. It revealed that the grain size of the SnO_2 films decreases as doping increases. The optical properties were studied with a UV-Vis spectrophotometer. The study showed that SnO_2 films had allowed direct transitions. The energy band gap varied from (3.5 to 3.55) eV with an increasing Mn_2O_3 doping ratio. The transmittance increased while the extinction coefficient (k) and the refractive index (n) decreased with the doping ratio increase. The behavior of the real ε_r and the imaginary ε_i part of the dielectric constant exhibited the same manner as n and k, respectively.

References

[1] A. Maab Abood and Bushra A. Hasan, "A Comparison Study the Effect of Doping by Ga_2O_3 and CeO_2 On the Structural and Optical Properties of SnO_2 Thin Films," *Iraqi Journal of Science*, vol. 64, no. 4, pp. 1675-1690, 2023.

[2] Ban K. Mohammed, "A Study of some the optical properties for (SnO_2) thin films prepared by Sol-Gel method,". *Iraqi Journal of Science*, vol. 58, no. 2B, pp. 848-859, 2017.

[3] M. Kafle, R. K. Kapadi , L. P. Joshi, and B. P. Kafle, "Effect of calcination environments and plasma treatment on structural, optical and electrical properties of FTO transparent thin films," *AIP Adv*, vol. 7, no. 7, pp. 1-10, 2017.

[4] H. S. Al-Jumali and A. Z. Al-Jenaby, "Structural and Optical Properties of Mn-Doped Tin Oxide Thin Films," *International Journal of Application or Innovation in Engineering & Management*, vol. 3, no. 9, pp. 139-144, 2014.

[5] G. H. Jihad, "Synthesis and Characterization of α-Fe_2O_3 Nanoparticles Prepared by PLD at Different Laser Energies," *Iraqi Journal of Science*, vol. 62, no. 11, pp. 3901-3910, 2021.

[6] J. Stankiewicz, X. Torrelles, J. L. García-Muñoz, and J. Blasco, "Structural and electrical properties of indium oxide thin films grown by pulsed laser deposition in oxygen ambient," *Journal of Alloys and Compounds*, vol. 694, pp. 1280-1286, 2017.

[7] H. Kim, R. C. Y. Auyeung, and A. Piqué, "Transparent conducting F-doped SnO2 thin films grown by pulsed laser deposition," *Thin Solid Films*, vol. 516, no. 15, pp. 1280-1286, 2008.

[8] H. Kim, R. C. Y. Auyeung, and A. Piqué, "F-doped SnO_2 thin films grown on flexible substrates at low temperatures by pulsed laser deposition," *Thin Solid Films*, vol. 520, no. 1, pp. 497-500, 2011.

[9] R. Kumar, "Hydrogen sulfide gas sensing properties of SnO_2 thin films prepared by thermal evaporation technique," *Journal of Physics: Conference Series*, vol. 1531, no. 1, p. 012013, 2020.

[10] M. Sharrouf, R. Awad, M. Roumié, and S. Marhaba, "Structural, Optical and Room Temperature Magnetic Study of Mn_2O_3 Nanoparticles," *Materials Sciences and Applications*, vol. 6, no. 10, pp. 1-10, 2015.

[11] J. S Sherin, M. Haris, D. Shiney Manoj, J. Koshy, and J.K. Thomas, "Enhanced electrochemical properties in nanostructured MnO_2, synthesized through a single step auto-igniting modified combustion technique," *International Journal of ChemTech Research*, vol. 10, no. 3, pp. 647–655, 2017

[12] N. S. Sabri, M. S. M. Deni, A. Zakaria, and M.K. Talari," Effect of Mn Doping on Structural and Optical Properties of SnO2 Nanoparticles Prepared by Mechanochemical Processing," *Physics Procedia*, vol. 25, pp. 233 – 239, 2012.

[13] A. Singh, A. Verma, and B. C. Yadav, "MnO_2- SnO_2 Based Liquefied Petroleum Gas Sensing Device for Lowest Explosion Limit Gas Concentration," *ECS Sensors Plus*, vol., no.1, pp. 2754-2726 ,2022.

[14] H. A. J. Hussien, R. G. Kadhim and A. Hashim," Investigating the low cost photodegradation performance against organic Pollutants using CeO_2/MnO_2/ polymer blend nanostructures," *Optical and Quantum Electronics*, vol. 54, article no.704, 2022.

[15] A. L. Patterson, "The Scherer Formula for X-Ray Particle Size Determination," *Physical review*, vol. 56, no. 10, pp. 978–982, 1939.

[16] M. O. Orlandi, P. R. Bueno, E. R. Leite, and E. Longo, "Nonohmic behavior of SnO2.MnO2-based ceramics," *Materials Research*, vol. 6, no. 2, pp. 279-283, 2003.

[17] B. G. Abead, M. H. Dwech, and K. A. Aadim, "Structural and Optical Properties of SnO2: MgO Thin Films Preparing by Pulse Laser Deposition Technique at 423K," *Journal of Kerbala University*, vol. 11, no. 1, pp. 293-302, 2015.

[18] S. M. Ali, S. T. Hussain, S. A. Bakar, J. Muhammad, and N. U. Rehman, "Effect of doping on the Structural and Optical Properties of SnO_2 Thin Films fabricated by Aerosol Assisted Chemical Vapor Deposition," *Journal of Physics: Conference Series*, vol. 439, no. 1, P. 012013, 2013.

[19] S. P. Sharma, and P. Sharma, "Effect of Annealing Temperature on Structural and Optical properties of Mn-doped SnO_2 Thin Films Prepared by Sol-Gel Technique," *International Journal of Scientific Research in Physics and Applied Sciences*, vol. 7, no. 2, pp. 99-107, 2019.

[20] N. S. Sabri, M. S. M. Deni, A. Zakaria, and M. K. Talari, "Effect of Mn Doping on Structural and Optical Properties of SnO_2 Nanoparticles Prepared by Mechanochemical Processing," *Phys Procedia*, vol. 25, no.1, pp. 233-239, 2012.

[21] B. Sathyaseelan, K. Senthilnathan, T. Alagesan, R. Jayavel, and K. Sivakumar, "A study on structural and optical properties of Mn- and Co-doped SnO_2 nanocrystallites," *Mater Chem Phys*, vol. 124, no. 2–3, pp. 1046-1050,2010.

[22] F. E. Ghodsi and J. Mazloom, "Optical, electrical and morphological properties of p-type Mn-doped SnO_2 nanostructured thin films prepared by sol-gel process," *Appl. Phys. A Mater Sci. Process*, vol. 108, no. 3, pp. 693-700, 2012.

[23] S. K. Sharma, P. Thakur, Shalendra Kumar, D. K. Shukla, N. B. Brookes, C. G. Lee, K. R. Pirota, B. H. Koo, and M. Knobel, "Room temperature ferromagnetism in Fe-doped CeO_2 thin films grown on $LaAlO_3$ (001)," *Thin Solid Films*, vol. 519, no. 1, pp. 410-413, 2010.

[24] B. A. Hasan and M. A. Kadhim, "Structure, morphology and optical properties of thermally evaporated Cu_2S thin films annealed at different temperatures," *AIP Conference Proceedings*, vol. 2144, no.1, p. 030021, 2019.

[25] Burstein, Elias. "Anomalous optical absorption limit in InSb." *Physical review*, Vol. 93, no. 3, p. 632, 1954.

[26] J.Tauc, "amorphous and liquid semiconductors", London and New York: plenum press, 1974.

[27] S. Senthilkumaar, K. Rajendran, S. Banerjee, T. K. Chini, and V. Sengodan, "Influence of Mn doping on the microstructure and optical property of ZnO," *Mater Sci. Semicond. Process*, vol. 11, no. 1, pp.6-12, 2008.

[28] B. A. Hasan and M. A. Kadhim, "Effect of Germanium Content on the Optical Constants of GexS1-xThin Films," *IOP Conference Series: Materials Science and Engineering*, vol. 928, no. 7, p. 072009, 2020.